ChemPubSoc Europe

DOI: 10.1002/cplu.201900317

CHEMPLUSCHEM Full Papers

SPECIAL ISSUE

A Solution-Processable *meso*-Phenyl-BODIPY-Based *n*-Channel Semiconductor with Enhanced Fluorescence Emission

Emrah Ozcan,[a] Mehmet Ozdemir,[b] Dongil Ho,[c] Yunus Zorlu,[a] Resul Ozdemir,[b] Choongik Kim,*[c] Hakan Usta,*[b] and Bunyemin Cosut*[a]

The molecular design, synthesis, and characterization of an acceptor-donor-acceptor (A-D-A) semiconductor BDY-Ph-2T-Ph-BDY comprising a central phenyl-bithiophene-phenyl π-donor and BODIPY π-acceptor end-units is reported. The semiconductor shows an optical band gap of 2.32 eV with a highly stabilized HOMO/LUMO (−5.74 eV/−3.42 eV). Single-crystal X-ray diffraction (XRD) reveals D–A dihedral angle of ca. 66° and strong intermolecular "C–H···π (3.31 Å)" interactions. Reduced π-donor strength, increased D–A dihedral angle, and restricted intramolecular D–A rotations allows for both good fluorescence efficiency ($\Phi_F = 0.30$) and *n*-channel OFET transport ($\mu_e =$ 0.005 $cm^2/V \cdot s$; $I_{on}/I_{off} = 10^4$–10^5). This indicates a much improved (6-fold) fluorescence quantum yield compared to the *meso*-thienyl BODIPY semiconductor BDY-4T-BDY. Photophysical studies reveal important transitions between locally excited (LE) and twisted intramolecular charge-transfer (TICT) states in solution and the solid state, which could be controlled by solvent polarity and nano-aggregation. This is the first report of such high emissive characteristics for a BODIPY-based *n*-channel semiconductor.

Introduction

π-Conjugated small molecules with photon absorption/emission properties have attracted great scientific and technological interest as semiconducting materials in organic photovoltaics (OPVs), field-effect transistors (OFETs), and light-emitting transistors (OLETs).[1–4] The delocalization of π-electron density over the entire molecular system is very critical to the electronic/photonic properties of molecular semiconductors.[5–9] In addition to their promising charge-transport and photophysical properties, the most favorable physical and chemical properties of π-conjugated small molecules are structural versatility, ease of synthesis-purification and fabrication, and synthetic (batch-to-batch) reproducibility.[10–13] Among various π-building blocks, 4,4-difluoro-4-bora-*3a,4a*-diaza-*s*-indacene (BODIPY) has recently attracted attention in the design of molecular semiconductors for optoelectronics.[14] In the past few decades, BODIPY-based small molecules have been studied as fluorescent switches/sensors, chemosensors, biochemical labels, and photodynamic therapy agents,[15–18] and they have shown remarkable photophysical properties such as high fluorescence quantum yield, large extinction coefficient, small Stokes shifts, high photostability, and tunable absorption/fluorescence profiles.[19] The recent optoelectronic applications of BODIPY π-systems include organic photovoltaics (OPVs),[20] dye-sensitized solar cells (DSSCs),[21] organic field-effect transistors (OFETs),[22] light harvesting,[23] and near-infrared absorption.[24] Owing to its highly π-electron deficient electronic structure resulting in an energetically stabilized frontier orbitals, BODIPY is one of the unique π-acceptor building blocks that could be synthesized and functionalized in a few steps. Thanks to its excellent structural properties including high π-core planarity, large dipole moment (μ ~ 3–4 D), good π-delocalization, and high solubility, BODIPY is an ideal building block to form solution-processable donor-acceptor (D-A) type *n*-channel semiconductor architectures.[25–28] In addition to these structural features, the electronic properties of BODIPY-based semiconductors are unique because the majority charge carrier is highly dependent on its π-architecture. While aromatic substitution on BODIPY's *meso*-position yields *n*-channel (electron-transporting) semiconductivity,[29] π-extension through 2,6-positions leads to hole-transport (*p*-channel) characteristics.[26] Facile synthetic modifications on BODIPY have been demonstrated to finely tune chemical/photophysical and charge-transport characteristics, which then allows the development of optimized BODIPY π-structures for specific optoelectronic applications such as OLETs and OPVs.[29,30] To this end, we have recently demonstrated that when *meso*-thienyl BODIPYs are used as π-acceptor end-units in acceptor-donor-acceptor (A-D-A) type π-architec-

[a] E. Ozcan, Prof. Y. Zorlu, Prof. B. Cosut
Department of Chemistry
Gebze Technical University
Gebze, Kocaeli (Turkey)
E-mail: bc@gtu.edu.tr
[b] Dr. M. Ozdemir, R. Ozdemir, Prof. H. Usta
Department of Materials Science and Nanotechnology Engineering
Abdullah Gül University
Kayseri (Turkey)
E-mail: hakan.usta@agu.edu.tr
[c] D. Ho, Prof. C. Kim
Department of Chemical and Biomolecular Engineering
Sogang University
Mapo-gu, Seoul (Republic of Korea)
E-mail: choongik@sogang.ac.kr

Supporting information for this article is available on the WWW under https://doi.org/10.1002/cplu.201900317

This article is part of a Special Issue on "π-Conjugated (Macro)molecules and their Applications".

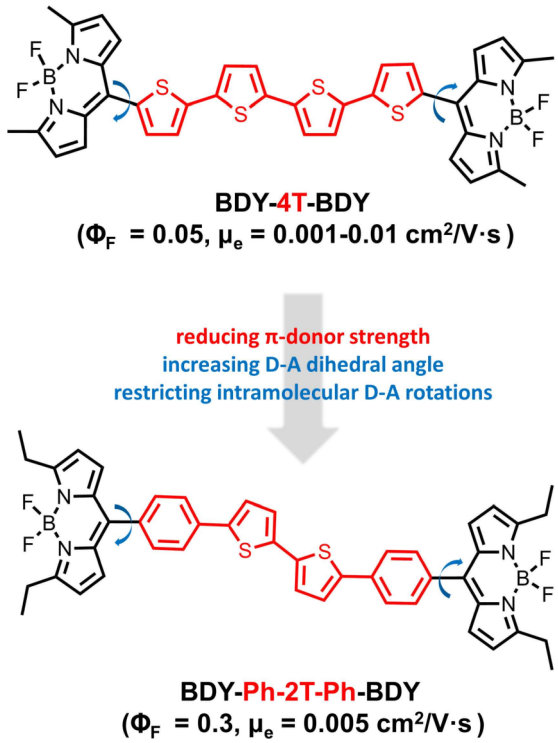

Figure 1. The chemical structures of BDY-Ph-2T-Ph-BDY developed in this study and the reference compound, BDY-4T-BDY, developed in our earlier study[31] showing π-donor (*in red*) and π-acceptor (*in black*) building blocks.

tures (e.g., BDY-4T-BDY, Figure 1), highly efficient electron-transport ($\mu_e \sim 0.001–0.01$ cm^2/V·s) characteristics in *n*-channel OFETs could be achieved.[31] In this design, we took advantage of the negative inductive (-*I*) and mesomeric (−*M*) effects provided by the BODIPY π-core, which enabled electron injection/stabilization/transport across the corresponding molecular solid-state. Despite all these recent efforts, there is still only a handful example of BODIPY-based *n*-channel semiconducting molecules reported for use in optoelectronics.[32] Furthermore, for the known BODIPY-based *n*-channel molecular semiconductors, emissive properties have either not been studied or reported to be very low as a result of strong D-A electronic structures. For instance, our previously reported high-performance small molecule BDY-4T-BDY showed meager fluorescence quantum yields ($\Phi_F \sim 0.04–0.05$).[31] Therefore, from a materials development/functionality standpoint, it is still precious to design and develop novel BODIPY-based semiconducting π-systems with improved photophysical properties. This way, good electron-transport characteristics and emissive properties could be simultaneously achieved to open new avenues for next-generation solution-processed optoelectronics.

In this study, we demonstrate the design, synthesis, and characterization of a new solution-processable A-D-A π-conjugated small molecule, BDY-Ph-2T-Ph-BDY (Figure 1), employing phenyl-bithiophene-phenyl (Ph-2T-Ph) central π-donor unit and BODIPY π-acceptor end units. The molecular design rationales used here are: (i) attaching BODIPY end units to the π-donor unit through *meso*-positions to facilitate electron-transport, (ii) decreasing π-donor strength (Ph-2T-Ph *vs.* 4T in BDY-4T-BDY) and (iii) increasing D-A dihedral angle/rotational barrier (BODIPY-Ph *vs.* BODIPY-T in BDY-4T-BDY) to minimize non-radiative decays and the formation of twisted intramolecular charge-transfer (TICT).[33–36] The new semiconductor shows a large dihedral angle (~66°) between BODIPY and *meso*-phenyl units and large local dipoles (μ = 3–4 D); both provide good solubility in common organic solvents. This solution processability enables convenient purification and thin-film fabrication for the new semiconductor. Also, the absence of long lipophilic substitution and the presence of significant local dipoles could lead to efficient intermolecular interactions favoring solid-state ordering. The new molecule was characterized by ^{1}H/^{13}C NMR, mass spectrometry, elemental analysis, and thermogravimetric analysis. The single-crystal structure of the key intermediate compound BDY-Ph-Br reveals crucial structural properties in the design of the new semiconductor. BDY-Ph-2T-Ph-BDY shows an optical band gap of 2.32 eV with highly stabilized HOMO/LUMO energies of −5.74 eV/−3.42 eV. BDY-Ph-2T-Ph-BDY was studied in solution-processed OFETs; it shows *n*-channel semiconductor behavior with electron mobility of 0.005 cm^2/V·s and I_{on}/I_{off} ratio of 10^4–10^5. The detailed photophysical characterizations show significant transitions between locally excited (LE) and twisted intramolecular charge-transfer (TICT) states via solvent polarity change and nano-aggregation. Significantly enhanced fluorescence characteristics (~6-fold increase in quantum yield) were achieved compared to the previously developed *n*-channel BODIPY semiconductors. To the best of our knowledge, this is the first time that such high emissive characteristics are reported for a BODIPY-based *n*-channel semiconductor. This is undoubtedly the result of rational molecular design employed here, which demonstrates an essential step towards the development of solution-processable highly fluorescent BODIPY-based *n*-channel semiconductors for next-generation optoelectronics.

Experimental Section

Materials and Methods

The reactions were carried out under N_2 unless otherwise noted by using Schlenk techniques. All reagents were obtained from commercial sources and used without any further purification unless otherwise noted. ^{1}H/^{13}C NMR characterizations were performed by a Bruker 400 spectrometer (^{1}H, 400 MHz; ^{13}C, 100 MHz). Elemental analyses were done by a LecoTruspec Micro model instrument. MALDI-TOF was performed by a Bruker Microflex LT MALDI-TOF-MS Instrument. Thermal properties of compounds were investigated by a Mettler Toledo TGA/SDTA 851 Thermogravimetric Analysis (TGA) Instrument and Differential Scanning Calorimeter DSC 821 equipped with METTLER TOLEDO STAR software at a heating rate of 10 °C/min under nitrogen. UV-Vis absorption and fluorescence emission measurements were performed by a Shimadzu, UV-1800 UV-Vis Spectrophotometer and Varian Eclipse spectrofluorometer,

respectively. The fluorescence quantum yield was determined in dichloromethane as compared to the fluorescence of Rhodamine 6G standard ($\Phi_F = 0.76$ in water). Electrochemistry was performed by a C3 cell stand electrochemical station equipped with BAS-Epsilon software (Bioanalytical Systems, Inc. Lafayette, IN). Dynamic light-scattering (DLS) measurements were performed on a Malvern, Nano ZS Zetasizer (Abdullah Gül University-Central Research Facility (AGU-CRF)). SEM images were taken using the ZEISS GeminiSEM 300 – Field Emission Scanning Electron Microscope at a 3 kV accelerating voltage (Abdullah Gül University-Central Research Facility (AGU-CRF)).

The Parameters for Fluorescence Quantum Yields

The fluorescence quantum yield values for BDY-4T-BDY and BDY-Ph-2T-Ph-BDY were determined in benzene by comparing to the fluorescence of Rhodamine 6G as a standard. Fluorescence quantum yields (Φ_F) were calculated by the comparative method [Equation (1)].[37]

$$\Phi F = \Phi_F(\mathrm{Std}) \frac{F.A_{Std}.n^2}{F_{Std}.A.n^2_{Std}} \quad (1)$$

where Φ_F(Std) is the fluorescence quantum yield of standard. Rhodamine 6G is employed as the standard ($\Phi_F = 0.76$ in water).[38] F and F_{Std} are the areas under the fluorescence emission curves of samples (BDY-4T-BDY and BDY-Ph-2T-Ph-BDY) and the standard, respectively. A and A_{Std} are the respective absorbance of the samples and standard at the excitation wavelengths. η^2 and η^2_{Std} are the refractive indices of solvents used for the sample and standard, respectively. The concentration of the solutions at the excitation wavelength was fixed at 1×10^{-5} M.

Synthesis and Characterization

The synthesis of BDY-4T-BDY was performed following our previously reported procedure.[31]

Synthesis of 8-(4-bromo-1-phenyl)-3,5-diethyl-4,4-difluoro-4-bora-3a,4a-diaza-s-indacene (BDY-Ph-Br): To a flask containing CH_2Cl_2 (300 ml), 4-bromobenzaldehyde (1150 mg, 6.25 mmol) and N-ethylpyrrole (1.3 mL, 12.5 mmol) were added, respectively, under nitrogen, followed by the addition of 3 drops of trifluoroacetic acid. The reaction mixture was stirred at room temperature for 12 h. Next, *p*-chloranil (1500 mg, 6.25 mmol) was added to the reaction medium, and the mixture was stirred at room temperature for an additional 30 min. Then, triethyl amine (5 mL) and boron trifluoride diethyl etherate ($BF_3.OEt_2$) (5 mL) were added, sequentially. The reaction mixture was stirred at room temperature for an additional 3 h. The reaction mixture was extracted with CH_2Cl_2 and water. Organic layer was dried with Na_2SO_4 and evaporated to dryness to give a crude product. The crude product was purified by silica gel column chromatography using CH_2Cl_2:Hexanes (3:1) as the eluent to give BDY-Ph-Br as a red solid (495 mg, 20% yield). ^{1}H NMR (400 MHz, $CDCl_3$): δ (ppm) 7.63–7.61 (d, J = 8.4 Hz, 2H), 7.37–7.35 (d, J = 8.4 Hz, 2H), 6.71–6.70 (d, J = 4.2 Hz, 2H), 6.36–6.35 (d, J = 4.2 Hz, 2H), 3.10–3.05 (q, J = 7.6 Hz, 4H), 1.36–1.33 (t, J = 7.6 Hz, 6H). ^{13}C NMR (100 MHz, $CDCl_3$): δ (ppm) 164.2, 141.4, 134.1, 133.2, 131.9, 131.6, 130.3, 124.6, 117.7, 22.2, 12.9. MS (MALDI-TOF) *m/z* $[M]^+$: calcd for $C_{19}H_{18}BBrF_2N_2$: 402.07; found: 402.280 $[M]^+$, 383.357 $[M–F]^+$.

Synthesis of 8,8′-([2,2′-bithiophene]-5,5′-diylbis(4,1-phenylene)) bis(3,5-diethyl-4,4-difluoro-4-bora-3a,4a-diaza-s-indacene) (BDY-Ph-2T-Ph-BDY): The solution of BDY-Ph-Br (150 mg, 0.372 mmol), 5,5′-bis(trimethylstannyl)-2,2′-bithiophene (89.2 mg, 0.181 mmol), and $Pd(PPh_3)_4$ (10.5 mg, 9.1 μmol) in anhydrous toluene (15 mL) was stirred at 110 °C for 24 hours. Then, the reaction mixture was allowed to warm to room temperature and evaporated to dryness to give a crude solid. The dark colored crude solid was isolated and washed with methanol; then, it was purified by silica gel column chromatography using CH_2Cl_2:Hexanes (2:1) as the eluent to afford BDY-Ph-2T-Ph-BDY as a dark red solid (112 mg, 73% yield). ^{1}H NMR (400 MHz, $CDCl_3$): δ (ppm) 7.73 (d, 2H, J = 8.0 Hz), 7.55 (d, 2H, J = 8.0 Hz), 7.39 (d, 1H, J = 4.0 Hz), 7.28 (d, 1H, J = 4.0 Hz), 6.83 (d, 2H, J = 4.0 Hz), 6.39 (d, 2H, J = 4.0 Hz), 3.08 (q, 4H, J = 22.8 Hz), 1.35 (t, 6H, J = 15.2 Hz). ^{13}C NMR (100 MHz, $CDCl_3$): δ (ppm) 163.6, 142.1, 137.5, 135.6, 134.1, 133.5, 131.2, 130.2, 125.2, 125.1, 124.9, 117.4, 22.1, 12.8. MS (MALDI-TOF) *m/z* $[M]^+$: calcd for $C_{46}H_{40}B_2F_4N_4S_2$: 810.28; found: 810.11$[M]^+$, 791.085 $[M–F]^+$. Elemental analysis calcd (%) for $C_{46}H_{40}B_2F_4N_4S_2$: C, 68.16; H, 4.97; N, 6.91; found: C, 67.89; H, 5.03; N, 7.01.

Field-Effect Transistor Fabrication and Characterization

Top contact/bottom gate (TC/BG) OFETs were fabricated on highly *n*-doped silicon wafers having thermally grown 300 nm oxide layer (areal capacitance; $C_i = 11.4$ nF cm^{-2}). The substrates were sonicated in acetone for 10 min and then treated with air plasma for 5 min (Harrick plasma, PDC-32G, 18 W). PS-brush ($M_w = 1.7$–28 kg mol^{-1}) treatments were implemented on the cleaned substrates following the conventional procedure.[39] The solution-shearing method was employed to form organic semiconductor layers on PS-brush-treated substrates where the concentration of the organic solution, solvent type, substrate temperature, and shearing speed were optimized. The substrates were placed in a vacuum oven to remove residual solvent. Finally, Au source and drain electrodes (40 nm) were thermally evaporated to define the semiconductor channel width (W) and length (L) of 1000 and 50 μm, respectively. Electrical characteristics of OFETs were measured in vacuum conditions at room temperature with a semiconductor parameter analyzer (Keithley 4200-SCS). The saturation charge-carrier mobility (μ_{sat}) for an OFET device was calculated in the saturation regime as the average value of at least 10 OFET devices using the formula:

$$\mu_{sat} = (2I_{DS}L)/[WC_i\ (V_G - V_{th})^2]$$

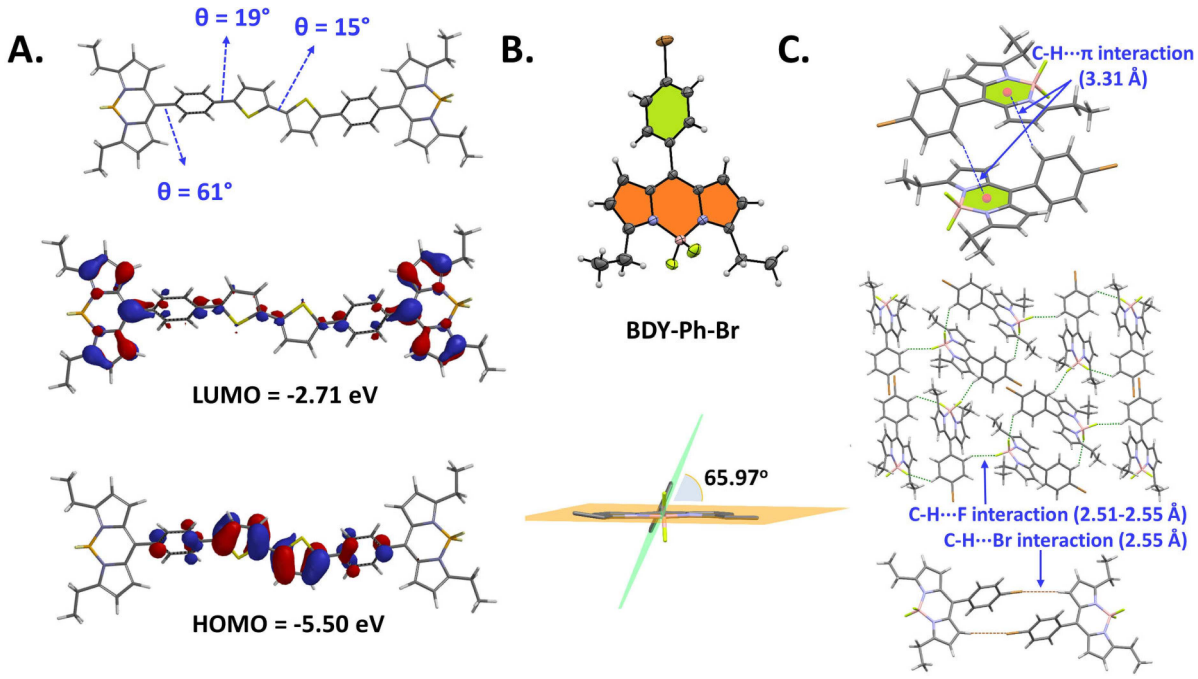

Figure 2. A. Optimized molecular geometry for BDY-Ph-2T-Ph-BDY showing inter-ring torsional angles (θ), computed HOMO/LUMO energies, and frontier molecular orbital topographies. B. X-ray single-crystal structure of BDY-Ph-Br with 50% ellipsoids and the perspective view of the inter-ring dihedral angle between "boron-dipyrromethene" and "*meso*-phenyl" π-units. (The grey, blue, pink, yellow, and white coloured atoms represent C, N, B, F, and H, respectively) C. The perspective views of the short "C–H···π", "C–H···Br", and "C–H···F" contacts. (CCDC 1876266 (BDY-Ph-Br) contains the supplementary crystallographic data for this paper, and these data can be obtained free of charge from The Cambridge Crystallographic Data Centre)

where I_{DS} is the source-drain current, L is the channel length, W is the channel width, C_i is the areal capacitance (11.4 nF·cm^{-2}) of the gate dielectric, V_G is the gate voltage, and V_{th} is the threshold voltage. The voltage ranges used in charge carrier mobility calculations are between 50–80 V. The thin-film microstructure and surface morphology were analyzed by atomic force microscopy (AFM, NX10, Park systems) and wide-angle X-ray diffraction (XRD, Ultima IV, Rigaku).

Results and Discussion

Computational Modeling, Synthesis, Characterization, and Single Crystal X-ray Analysis

The density functional theory (DFT) calculations performed at the B3LYP/6-31G**[40] level of theory indicates that the central Ph-2T-Ph π-donor unit in BDY-Ph-2T-Ph-BDY is coplanar with small inter-ring dihedral angles of ~15–19° (Figure 2A). This angle is below the threshold value of torsional angle (~30–35°) at which π-conjugation breaks,[41] and it provides a very efficient π-orbital delocalization through the donor unit. Indeed, the HOMO completely delocalizes on this π-donor framework with no contribution from BODIPY acceptor π-system. On the other hand, sizeable inter-ring dihedral angle of ~61° is calculated between "boron-dipyrromethene" and "*meso*-phenyl" π-units, which matches well with the single-crystal structure of the BDY-Ph-Br intermediate compound (Figure 2B). As a result of this mostly broken π-conjugation between donor and acceptor units, the LUMO has significantly larger electron densities on the terminal BODIPY π-acceptors with minimal contributions from phenyl/thienyl units. The HOMO and LUMO energies for BDY-Ph-2T-Ph-BDY were calculated to be −5.50 eV and −2.71 eV, respectively, which are relatively higher than those calculated for the reference compound BDY-4T-BDY (E_{HOMO}/E_{LUMO} = −5.58/−3.17 eV). The nonsymmetric increase in frontier orbital energies results in increased HOMO-LUMO energy gap for the new compound ($E_{HOMO\text{-}LUMO}$ for BDY-Ph-2T-Ph-BDY = 2.79 eV) as compared with BDY-4T-BDY ($E_{HOMO\text{-}LUMO}$ = 2.41 eV), most likely a result of lowered π-donor strength (Ph-2T-Ph *vs.* 4T) and increased dihedral twist (Ph-BDY *vs.* T-BDY) between donor and acceptor units.

The synthetic route to BDY-Ph-2T-Ph-BDY is outlined in Scheme 1. In order to prevent potential instability of the dipyrromethene π-core, the BODIPY structure employed in this study is synthesized bearing two ethyl substituents at α-positions. BDY-Ph-Br was synthesized in 20% yield by first reacting 4-bromobenzaldehyde with 2-ethyl pyrrole in the presence of catalytic amount of trifluoroacetic acid, followed by oxidization with tetrachloro-*p*-benzoquinone and coordination with trifluoroborane-dietherate ($BF_3.OEt_2$) in the presence of *N,N*-diisopropylethylamine. BDY-Ph-2T-Ph-BDY was synthesized via Stille cross-coupling reaction between BDY-Ph-Br and 5,5′-bis(trimethylstannyl)-2-2′-bithiophene in the presence of tetrakis(triphenylphosphine)palladium(0) catalysts in toluene at 110 °C. The good solubility of the target compound, BDY-Ph-2T-Ph-BDY, enabled convenient purification via column chromatography (silica gel/CH_2Cl_2:Hexanes (2:1)), and the pure product

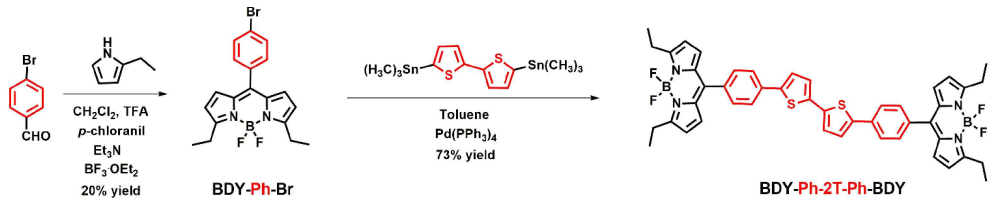

Scheme 1. Synthetic route to BDY-Ph-2T-Ph-BDY.

was obtained as a dark red solid in 73% yield. Consistent with the previously developed BODIPY semiconductors, BDY-Ph-2T-Ph-BDY's A-D-A π-system is found to be highly soluble in common organic solvents despite the absence of long lipophilic alkyl substituents. This points to the combined effects of large molecular dipoles of BODIPY units and increased inter-ring torsions between D and A units enhancing interactions with the solvent molecules. The chemical structures and purities of BDY-Ph-Br and BDY-Ph-2T-Ph-BDY were established by $^{1}H/^{13}C$ NMR (Figures S1, S2, S4, S5), MALDI-TOF mass spectrometry (MS) (Figures S3 and S6), and elemental analysis. The thermogravimetric analysis (TGA) (10 °C min^{-1} heating rate, under nitrogen) of the new molecule indicates excellent thermal stability with the decomposition onset (5% mass loss) temperature at 367 °C (Figure S7). However, standard melting temperature measurement and differential scanning calorimetry (DSC) analysis did not show any thermal transition prior to the molecular decomposition.

Although single-crystals of the final molecular structure, BDY-Ph-2T-Ph-BDY, could not be obtained, red crystals of the intermediate compound BDY-Ph-Br (Scheme 1) suitable for single-crystal analysis were grown by diffusion of hexane into a chloroform solution at room temperature (Figure 2). BDY-Ph-Br crystallizes in the monoclinic $P2_1/n$ space group, and the solid-state structure reveals highly coplanar "boron-dipyrromethene" core (C_9BN_2) subunit with two ethyl groups ($-C_2H_5$) lying nearly in the same plane with tilt angles of 1.57° and 9.16°. The "B–F" bond distances and "F–B–F", "N–B–N", and "N–N–F" bond angles match closely with those of previously reported BODIPY-based π-conjugated small molecules[31,42] As shown in Figure 2B, the dihedral angle between the *meso*-phenyl group and the boron-dipyrromethene π-core was found to be 65.97°, which matches well with the computationally optimized geometries. This angle is large as compared to that of *meso*-thiophene substituted BODIPY ($\theta_{dihedral} = 48.8°$) in BDY-4T-BDY, which doubtless reflects sterically encumbered nature of the six-membered phenyl ring having "C–H" bonds pointing towards the BODIPY's 1,7-positions. Note that this observed dihedral angle is in the range of those previously reported *meso*-phenyl substituted BODIPY small molecules[43,44] Although π-π stacking interactions in the solid-state are not effective showing relatively large centroid-to-centroid distances of > 4.6 Å, strong "C–H···π" (3.31 Å) interactions and short "C–H···Br" (2.55 Å ≪ $r_{vdw}(Br) + r_{vdw}(H) = 3.09$ Å) and "C–H···F" (2.51–2.55 Å ≪ $r_{vdw}(F) + r_{vdw}(H) = 2.67$ Å) contacts are found to play key roles in forming three-dimensional crystal packing (Figure 2C). Specifically, "C–H···π" interactions (*herringbone-type packing*) between aromatic moieties of the final π-structure could be quite advantageous for two-dimensional charge transport in BDY-Ph-2T-Ph-BDY thin-film.

Optical and Electrochemical Properties

The optical properties and electronic structure of the new small molecule were studied by optical absorption/fluorescence spectroscopies and cyclic voltammetry. As shown in Figure 3A, BDY-Ph-2T-Ph-BDY shows an absorption maximum at 512 nm with the out-of-plane vibronic features at 484/451 nm (1129/2641 cm^{-1} from the maximum). This is the unique absorption profile of *meso*-aromatic BODIPY's π-π* transition ($S_0 \rightarrow S_1$).[45] The optical band gap is estimated as 2.32 eV from the low energy absorption onset. When compared with the reference compound BDY-4T-BDY ($\lambda_{max} = 526$ nm, $E_g^{opt} = 2.19$ eV), the absorption maximum for BDY-Ph-2T-Ph-BDY shifts to higher energy and the optical band gap increases. This reflects the combined effects of lowered π-donor strength (Ph-2T-Ph *vs.* 4T) and increased dihedral angle (lowered π-conjugation) between *meso*-aromatic and BODIPY moieties (~66° for phenyl *vs.* ~49° for thienyl) in the new molecule. UV-Vis absorption spectra of the corresponding solution-processed BDY-Ph-2T-Ph-BDY thin-film exhibits a significantly red-shifted absorption profile with the maximum located at 542 nm. The solid-state optical band gap is estimated as 2.11 eV. This result points to intramolecular π-core planarization and enhanced intermolecular interactions in BDY-Ph-2T-Ph-BDY's solid-state, which is consistent with the observed thin-film crystallinity (*vide infra*). Cyclic voltammetry measurement in THF solution shows a reversible reduction for

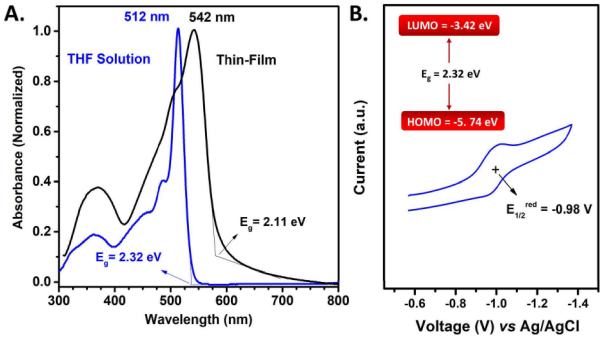

Figure 3. A. Optical absorption spectra of BDY-Ph-2T-Ph-BDY in THF solution (1×10^{-5} M) and as thin-film, and the corresponding optical band gaps (E_g). B. Cyclic voltammogram of BDY-Ph-2T-Ph-BDY in THF (0.1 M $Bu_4N^+PF_6^-$, scan rate = 50 mV·s^{-1}) and experimental HOMO-LUMO energy levels.

BDY-Ph-2T-Ph-BDY with the half-wave potential ($E_{1/2}^{red}$) located at −0.98 V (*vs* Ag/AgCl). This indicates a stable *n*-doping/undoping characteristics with a low LUMO energy level of −3.42 eV for BDY-Ph-2T-Ph-BDY. The HOMO energy level is estimated as low as −5.74 eV. Based on the frontier orbital energetics and electrochemical behavior, it is evident that BDY-Ph-2T-Ph-BDY is a potential *n*-channel semiconductor in field-effect transistors.

The fluorescence properties of the new molecule were explored by both steady-state and time-resolved fluorescence spectroscopy techniques. Although the absorption profile of the new molecule remains nearly the same ($\Delta\lambda_{max}$ ~3–4 nm) in several solvents of different polarity (Figure 4A), the corresponding fluorescence spectra show dramatic changes upon polarity increase (Figure 4B). This indicates that the ground-state of BDY-Ph-2T-Ph-BDY has much less polarity than the excited state. The fluorescence spectrum of BDY-Ph-2T-Ph-BDY (1×10^{-5} M in solution, λ_{exc} = 510 nm) shows a single sharp emission peak λ_{max} located at 536–538 nm (Stokes shift ~25 nm) in a low polarity solvent (e.g., 1,4-dioxane and toluene). When the fluorescence spectrum is taken in a more polar medium (e.g., chloroform, dichloromethane, THF), the intensity of the emission peak at higher energy significantly decreases, and a new broad highly red-shifted (Stokes shift ~103–138 nm) emission peak appears with λ_{max} located at 615–660 nm. Based on these fluorescence characteristics, while the higher energy peak is attributed to a locally excited (LE) state, lower energy peak originates from a twisted intramolecular charge transfer (TICT) state.[33,34,46] The higher wavelength peak shows a pronounced solvatochromism indicating energetic stabilization of polar TICT state in polar solvents. To further explore the effect of medium polarity on fluorescence characteristics of BDY-Ph-2T-Ph-BDY, the emission measurements were carried out by admixing nonpolar toluene and polar THF at different ratios. As shown in Figure 4C, reduction of solvent polarity by gradual addition of toluene into THF solution (volume fraction: from 0 to 100%) progressively increases the intensity of the emission peak at higher energy (~536 nm) and decreases the lower energy emission peak intensity along with a hypsochromic shift (λ_{em} = 635 nm→613 nm). In solvent mixtures of >30% toluene, the higher energy peak exhibits higher intensities relative to the lower energy peak and eventually becomes the only peak observed in the emission spectra in pure toluene. All these observations corroborate the assignments of LE and TICT states for BDY-Ph-2T-Ph-BDY.

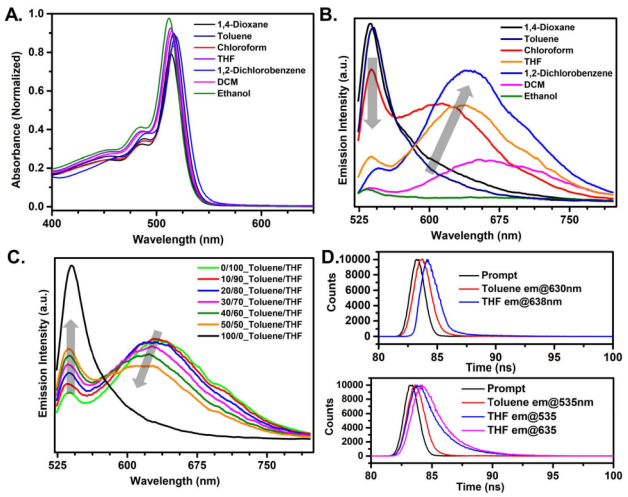

Figure 4. (A, B) Optical absorption and fluorescence emission spectra of BDY-Ph-2T-Ph-BDY in solvents with varied polarities. (C) Fluorescence emission spectra of BDY-Ph-2T-Ph-BDY in toluene/THF mixtures (solution concentration = 1×10^{-5} M; excitation wavelength = 510 nm). (D) Fluorescence decay plots along with fitted data for BDY-4T-BDY (top curve) and BDY-Ph-2T-Ph-BDY (bottom curve) solutions in THF and toluene upon excitation at 390 nm.

These fluorescence characteristics are in sharp contrast to those of BDY-4T-BDY that exhibits only broad emission peaks with highly red-shifted (Stokes shift ~104–152 nm) maxima at 630/678 nm (in Toluene/THF) with no observable high-energy emission (Figure S8). Therefore, BDY-4T-BDY fluorescence seems to originate only from a twisted intramolecular charge transfer (TICT) state. These observations clearly indicate that highly emissive locally excited (LE) state becomes more effective in the new molecule while non-radiative decay pathways are minimal as a result of increasing D-A dihedral angle (~66° for *meso*-phenyl vs. ~49° for *meso*-thienyl), reducing π-donor strength (Ph-2T-Ph vs. 4T), and restricting intramolecular D-A rotations (higher rotational barrier for *meso*-phenyl vs. *meso*-thienyl).[35,36] However, note that higher polarity medium is still found to facilitate LE-state→TICT-state transition in the new molecular structure, and concurrent emissions from both emissive states could be observed in relatively polar solvents (Figures 4B and 4 C).[34] The fluorescence quantum yield (Φ_F) and lifetime (τ_F) measurements point to improved fluorescence characteristics in the new molecular design, and they align well with the proposed fluorescence mechanisms. Much larger quantum yields of 0.30/0.25 (in THF/Toluene) are measured for BDY-Ph-2T-Ph-BDY indicating ~6-fold increase compared to the reference compound BDY-4T-BDY (Φ_F = 0.053/0.055 in THF/Toluene). Also, fluorescence lifetimes of 1.72 ns (λ_{em} = 535 nm) and 1.84 ns (λ_{em} = 635 nm) are measured in THF for BDY-Ph-2T-Ph-BDY, which are much larger than those of BDY-4T-BDY (0.4–0.5 ns) (Figure 4D and Table S3). Furthermore, BDY-Ph-2T-Ph-BDY exhibits much shorter lifetime of 0.40 ns (λ_{em} = 535 nm) in toluene since the emission originates only from LE state with no contribution of charge-transfer.

BDY-Ph-2T-Ph-BDY also demonstrates aggregation induced emission (AIE) behavior, which – when combined with charge-transport properties – has been very crucial to design novel photonic applications.[47,48] The AIE behavior was studied by adding a nonsolvent (water) to a well-dissolved solution of the new molecule in THF. As shown in Figure 5A, upon increasing water volume fraction from 0% to 25%, the lower energy emission peak initially shows a bathochromic shift of ~40–50 nm as a result of the energetic stabilization of the TICT state due to the effect of polarity increase. The fluorescence intensity is observed to be severely quenched at the same time. When nonsolvent water volume fraction further increases to 50–70% yielding a low-solubility environment for BDY-Ph-2T-Ph-BDY, hypsochromic shift (~30–40 nm) of the lower energy maximum was observed along with a significant fluorescence intensity

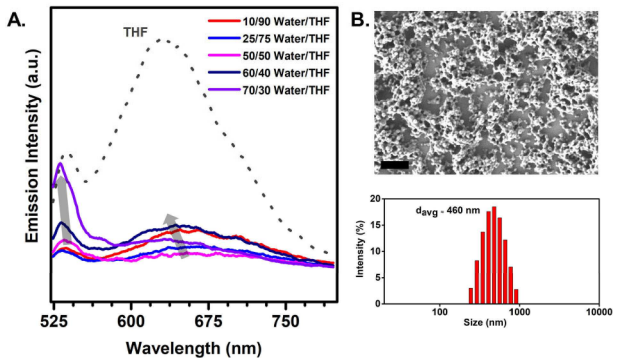

Figure 5. (A) Fluorescence emission spectra of BDY-Ph-2T-Ph-BDY in water/THF mixtures (solution concentration = 1×10^{-5} M; excitation wavelength = 510 nm). Arrows indicate the spectral changes upon nonsolvent water addition. (B) The size distribution of the nano-aggregates in water/THF (70:30, v/v) solution determined by dynamic light-scattering (DLS) and the SEM image of the BDY-Ph-2T-Ph-BDY nanoparticles/aggregates as film drop-cast on Si(100) from the same solution. Scale bar: 1 μm.

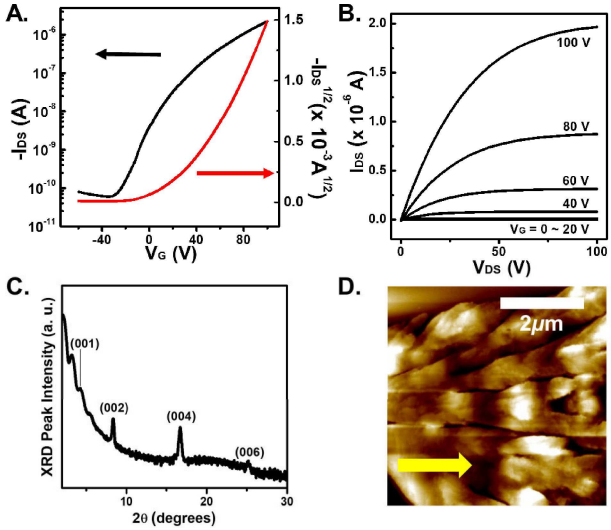

Figure 6. Representative transfer (A) and output (B) curves for *n*-channel OFETs based on solution-sheared BDY-Ph-2T-Ph-BDY semiconductor layer. θ-2θ XRD scan (C) and AFM topographic image (5×5 μm^2) of solution-sheared BDY-Ph-2T-Ph-BDY thin-film. The arrow shows the shearing direction.

increase in the higher energy peak at 536 nm. This obviously reveals that BDY-Ph-2T-Ph-BDY molecules transform into solid-state forming nano-aggregates, which leads to restricted intramolecular D-A rotations and reduced medium polarity around the molecules.[33,49] As a result, LE emission becomes dominant with minimal contribution from the TICT state. Dynamic Light-Scattering (DLS) measurement in water/THF (70:30, v/v) solution confirms the formation of BDY-Ph-2T-Ph-BDY nano-aggregates in sizes of ~200–900 nm (d_{avg} ~460 nm) (Figure 5B). The scanning electron microscope (SEM) image (Figure 5B) of the corresponding drop-casted film prepared from this solution on Si(100) shows a 3D network morphology of micron-sized aggregates that consist of nearly spherical BDY-Ph-2T-Ph-BDY nanoparticles (~200–600 nm), which is consistent with the DLS particle size distribution.

Thin-Film Microstructure/Morphology and Field-Effect Transistor Characterization

The charge transport characteristics of the new BODIPY small molecule was studied in top-contact/bottom-gate (TC/BG) OFET devices by solution-shearing BDY-Ph-2T-Ph-BDY solution (1 mg/mL in chlorobenzene) on PS-brush treated n^{++}-Si/SiO_2 substrates. The microstructure and surface morphology of the solution-sheared BDY-Ph-2T-Ph-BDY thin-film were characterized by θ-2θ X-ray diffraction (XRD) measurement and atomic force microscopy (AFM). XRD scans for the semiconductor thin-film showed multiple peaks for the same diffraction family up to the sixth-order suggesting a reasonably crystalline microstructure (Figure 6C). The primary diffraction peak (001) was observed at $2\theta = 4.26°$ corresponding to *d*-spacing of 20.7 Å, which is smaller than the computed molecular length (28.8 Å) of BDY-Ph-2T-Ph-BDY. Therefore, it is very probable that the semiconductor molecules adopt tilted edge-on orientation on the surface with a ~44° tilting angle from the substrate normal. As shown in Figure 6D, AFM characterization reveals the presence of micrometer-sized crystalline domains aligned along the shearing direction. The OFET devices were completed by thermally evaporation of Au source-drain electrodes on the semiconductor layer. OFETs demonstrated typical *n*-channel transistor characteristics under vacuum with appreciable electron mobility of 0.0054 cm^2/V·s and I_{on}/I_{off} ratio of 3.7×10^4 (Figures 6A and B), which correlate well with BDY-Ph-2T-Ph-BDY's computed/measured electronic structure and the observed solid-state microstructure/morphology. The semiconducting performance of BDY-Ph-2T-Ph-BDY is among the highest of previously reported *n*-channel BODIPY semiconductors (μ_e ~ 10^{-4}–0.01 cm^2/V·s).[14] The small decrease in electron mobility, as compared with the best results of BDY-4T-BDY (μ_e = 0.01 cm^2/V·s), could be attributed to increased LUMO energy level, narrower π-delocalization, and increased D-A backbone twist in the new molecular structure. Increasing D-A backbone twists lead to a decrease in effective π-conjugation and charge carrier π-delocalization across the molecular backbone, which results in slightly lowered charge-transport characteristics for the new molecule.[41] Increased emissive properties of the new molecule could be combined with its appreciable electron mobility to enable novel photonic applications.

Conclusion

We have described the molecular design, synthesis, and characterization of a new acceptor-donor-acceptor (A-D-A) semiconductor BDY-Ph-2T-Ph-BDY comprising a central phenyl-bithiophene-phenyl π-donor and BODIPY π-acceptor end-units. Single-crystal X-ray diffraction (XRD) analysis of the key intermediate compound BDY-Ph-Br shows an increased D-A dihedral angle of ~66° and strong intermolecular "C–H···π (3.31 Å)" interactions. BDY-Ph-2T-Ph-BDY exhibits an optical

band gap of 2.32 eV with highly stabilized HOMO and LUMO energies of −5.74 eV and −3.42 eV, respectively. Detailed photophysical studies reveal important transitions between locally excited (LE) and twisted intramolecular charge-transfer (TICT) states in solution and solid-state, which could be controlled by solvent polarity and nano-aggregation. Restricted intramolecular D-A rotations, reduced π-donor strength, and increased D-A dihedral angle allows for both good fluorescence efficiency ($\Phi_F = 0.30$) and *n*-channel OFET transport ($\mu_e = 0.005\ cm^2/V \cdot s$; $I_{on}/I_{off} = 10^4$–10^5) for BDY-Ph-2T-Ph-BDY, which indicates a much improved (~6-fold) fluorescence quantum yield compared to *meso*-thienyl BODIPY semiconductor BDY-4T-BDY. To the best of our knowledge, considering its electron mobility and emission characteristics, BDY-Ph-2T-Ph-BDY is among the highest performing BODIPY-based emissive *n*-type small molecules. Undoubtedly, our results provide important guidelines towards designing solution-processable highly fluorescent BODIPY-based molecular semiconductors for next-generation organic optoelectronics.

Supporting Information

Chemical characterizations (^{1}H NMR/^{13}C NMR/MALDI TOF-MS spectra) for BDY-Ph-Br and BDY-Ph-2T-Ph-BDY; thermogravimetric analysis (TGA) of BDY-Ph-2T-Ph-BDY; single crystal structure data and structure refinement details for BDY-Ph-Br; fluorescence emission spectra of BDY-4T-BDY in toluene and THF solutions are given in the Supporting Information.

Acknowledgements

H.U. acknowledges support from the Scientific and Technological Research Council of Turkey (TUBITAK) grant number of 114 M226. This research was supported by the National Research Foundation of Korea grant funded by the Korean government (MSIT) (NRF-2017R1A2B4001955).

Conflict of Interest

The authors declare no conflict of interest.

Keywords: acceptor-donor-acceptor compounds · BODIPY · fluorescence · organic field-effect transistors · organic semiconductors

[1] M. Ozdemir, S. Genc, R. Ozdemir, Y. Altintas, M. Citir, U. Sen, E. Mutlugun, H. Usta, *Synth. Met.* **2015**, *210*, 192–200.
[2] X. Guo, R. P. Ortiz, Y. Zheng, M.-G. Kim, S. Zhang, Y. Hu, G. Lu, A. Facchetti, T. J. Marks, *J. Am. Chem. Soc.* **2011**, *133*, 13685–13697.
[3] K. Yang, Q. Liao, C. W. Koh, J. Chen, M. Su, X. Zhou, Y. Tang, Y. Wang, Y. Zhang, H. Y. Woo, X. Guo, *J. Mater. Chem. A* **2019**, *7*, 9822–9830.
[4] C. Ruiz, I. Arrechea-Marcos, A. Benito-Hernández, E. Gutierrez-Puebla, M. A. Monge, J. T. López Navarrete, M. C. Ruiz Delgado, R. P. Ortiz, B. Gómez-Lor, *J. Mater. Chem. C* **2018**, *6*, 50–56.
[5] R. Ozdemir, S. Park, İ. Deneme, Y. Park, Y. Zorlu, H. A. Alidagi, K. Harmandar, C. Kim, H. Usta, *Org. Chem. Front.* **2018**, *5*, 2912–2924.
[6] M. Ozdemir, D. Choi, G. Kwon, Y. Zorlu, H. Kim, M.-G. G. Kim, S. Y. Seo, U. Sen, M. Citir, C. Kim, H. Usta, *RSC Adv.* **2015**, *6*, 212–226.
[7] M. Sawamoto, M. J. Kang, E. Miyazaki, H. Sugino, I. Osaka, K. Takimiya, *ACS Appl. Mater. Interfaces* **2016**, *8*, 3810–3824.
[8] R. Ponce Ortiz, H. Herrera, M. J. Mancheño, C. Seoane, J. L. Segura, P. Mayorga Burrezo, J. Casado, J. T. Lõpez Navarrete, A. Facchetti, T. J. Marks, *Chem. Eur. J.* **2013**, *19*, 12458–12467.
[9] L. Zhang, A. Fonari, Y. Liu, A. L. M. Hoyt, H. Lee, D. Granger, S. Parkin, T. P. Russell, J. E. Anthony, J. L. Brédas, V. Coropceanu, A. L. Briseno, *J. Am. Chem. Soc.* **2014**, *136*, 9248–9251.
[10] H. Ebata, T. Izawa, E. Miyazaki, K. Takimiya, M. Ikeda, H. Kuwabara, T. Yui, *J. Am. Chem. Soc.* **2007**, *129*, 15732–15733.
[11] R. Capelli, S. Toffanin, G. Generali, H. Usta, A. Facchetti, M. Muccini, *Nat. Mater.* **2010**, *9*, 496–503.
[12] S. Allard, M. Forster, B. Souharce, H. Thiem, U. Scherf, *Angew. Chem. Int. Ed.* **2008**, *47*, 4070–4098.
[13] T. Izawa, E. Miyazaki, K. Takimiya, *Adv. Mater.* **2008**, *20*, 3388–3392.
[14] D. Ho, R. Ozdemir, H. Kim, T. Earmme, H. Usta, C. Kim, *ChemPlusChem* **2019**, *84*, 18–37.
[15] A. C. Benniston, G. Copley, A. Harriman, R. Ryan, *J. Mater. Chem.* **2011**, *21*, 2601–2608.
[16] S. O. Tümay, E. Okutan, I. F. Sengul, E. Özcan, H. Kandemir, T. Doruk, M. Çetin, B. Çoşut, *Polyhedron* **2016**, *117*, 161–171.
[17] L. Huang, Z. Li, Y. Zhao, Y. Zhang, S. Wu, J. Zhao, G. Han, *J. Am. Chem. Soc.* **2016**, *138*, 14586–14591.
[18] Y. Wang, F. Pan, Y. Zhang, F. Peng, Z. Huang, W. Zhang, W. Zhao, *Analyst* **2016**, *141*, 4789–4795.
[19] G. Ulrich, R. Ziessel, A. Harriman, *Angew. Chem. Int. Ed.* **2008**, *47*, 1184–1201.
[20] B. Kim, B. Ma, V. R. Donuru, H. Liu, J. M. J. Fréchet, *Chem. Commun.* **2010**, *46*, 4148–4150.
[21] S. Kolemen, O. A. Bozdemir, Y. Cakmak, G. Barin, S. Erten-Ela, M. Marszalek, J. H. Yum, S. M. Zakeeruddin, M. K. Nazeeruddin, M. Grätzel, E. U. Akkaya, *Chem. Sci.* **2011**, *2*, 949–954.
[22] B. C. Popere, A. M. Della Pelle, S. Thayumanavan, *Macromolecules* **2011**, *44*, 4767–4776.
[23] E. T. Eçik, E. Özcan, H. Kandemir, I. F. Sengul, B. Çoşut, *Dyes Pigm.* **2017**, *136*, 441–449.
[24] Y. Kubo, Y. Minowa, T. Shoda, K. Takeshita, *Tetrahedron Lett.* **2010**, *51*, 1600–1602.
[25] A. Bessette, G. S. Hanan, *Chem. Soc. Rev.* **2014**, *43*, 3342–3405.
[26] H. Usta, M. D. Yilmaz, A. J. Avestro, D. Boudinet, M. Denti, W. Zhao, J. F. Stoddart, A. Facchetti, *Adv. Mater.* **2013**, *25*, 4327–4334.
[27] R. Ozdemir, D. Choi, M. Ozdemir, G. Kwon, H. Kim, U. Sen, C. Kim, H. Usta, *J. Mater. Chem. C* **2017**, *5*, 2368–2379.
[28] R. Ozdemir, D. Choi, M. Ozdemir, H. Kim, S. T. Kostakoğlu, M. Erkartal, H. Kim, C. Kim, H. Usta, *ChemPhysChem* **2017**, *18*, 850–861.
[29] A. M. Poe, A. M. Della Pelle, A. V. Subrahmanyam, W. White, G. Wantz, S. Thayumanavan, *Chem. Commun.* **2014**, *50*, 2913–2915.
[30] A. Loudet, K. Burgess, *Chem. Rev.* **2007**, *107*, 4891–4932.
[31] M. Ozdemir, D. Choi, G. Kwon, Y. Zorlu, B. Cosut, H. Kim, A. Facchetti, C. Kim, H. Usta, *ACS Appl. Mater. Interfaces* **2016**, *8*, 14077–14087.
[32] T. Bura, N. Leclerc, S. Fall, P. Lévêque, T. Heiser, P. Retailleau, S. Rihn, A. Mirloup, R. Ziessel, *J. Am. Chem. Soc.* **2012**, *134*, 17404–17407.
[33] R. Hu, E. Lager, A. Aguilar-Aguilar, J. Liu, J. W. Y. Lam, H. H. Y. Sung, I. D. Williams, Y. Zhong, K. S. Wong, E. Peña-Cabrera, B. Z. Tang, *J. Phys. Chem. C* **2009**, *113*, 15845–15853.
[34] S. Sasaki, G. P. C. Drummen, G. Konishi, *J. Mater. Chem. C* **2016**, *4*, 2731–2743.
[35] K. K. Neena, P. Thilagar, *ChemPlusChem* **2016**, *81*, 955–963.
[36] J. H. Gibbs, L. T. Robins, Z. Zhou, P. Bobadova-Parvanova, M. Cottam, G. T. McCandless, F. R. Fronczek, M. G. H. Vicente, *Bioorg. Med. Chem.* **2013**, *21*, 5770–5781.
[37] S. Fery-Forgues, D. Lavabre, *J. Chem. Educ.* **1999**, *76*, 1260–1264.
[38] J. Olmsted, *J. Phys. Chem.* **1979**, *83*, 2581–2584.
[39] S. H. Park, H. S. Lee, J.-D. Kim, D. W. Breiby, E. Kim, Y. D. Park, D. Y. Ryu, D. R. Lee, J. H. Cho, *J. Mater. Chem.* **2011**, *21*, 15580–15586.
[40] M. M. J. Frisch, G. W. Trucks, H. B. Schlegel, G. E. Scuseria, H. A. Robb, J. R. Cheeseman, G. Scalmani, V. Barone, B. Mennucci, G. A. Petersson, J. L. Nakatsuji, M. Caricato, X. Li, H. P. Hratchian, A. F. Izmaylov, J. Bloino, G. Zheng, T. Sonnenberg, M. Hada, M. Ehara, K. Toyota, R. Fukuda, J. Hasegawa, M. Ishida, F. Nakajima, Y. Honda, O. Kitao, H. Nakai, T. Vreven, J. A. Montgomery, Jr., J. E. Peralta, R. Ogliaro, M. Bearpark, J. J. Heyd, E.

Brothers, K. N. Kudin, V. N. Staroverov, J. Kobayashi, J. Normand, K. Raghavachari, A. Rendell, J. C. Burant, S. S. Iyengar, C. Tomasi, M. Cossi, N. Rega, J. M. Millam, M. Klene, J. E. Knox, J. B. Cross, V. Bakken, C. Adamo, J. Jaramillo, R. Gomperts, R. E. Stratmann, O. Yazyev, A. J. Austin, R. Cammi, P. Pomelli, J. W. Ochterski, R. L. Martin, K. Morokuma, V. G. Zakrzewski, G. A. Voth, P. Salvador, J. J. Dan-nenberg, S. Dapprich, A. D. Daniels, D. Farkas, J. B. Foresman, J. V. Ortiz, J. Cioslowski, D. J. Fox, **2010**, Gaussian, Inc., Wallingford CT.

[41] J. L. Brédas, G. B. Street, B. Thémans, J. M. André, *J. Chem. Phys.* **1985**, *83*, 1323–1329.

[42] D. Aydin Tekdaş, G. Viswanathan, S. Zehra Topal, C. Y. Looi, W. F. Wong, G. Min Yi Tan, Y. Zorlu, A. G. Gürek, H. B. Lee, F. Dumoulin, *Org. Biomol. Chem.* **2016**, *14*, 2665–2670.

[43] B. Basumatary, A. Raja Sekhar, R. V. Ramana Reddy, J. Sankar, *Inorg. Chem.* **2015**, *54*, 4257–4267.

[44] S. Rihn, P. Retailleau, N. Bugsaliewicz, A. De Nicola, R. Ziessel, *Tetrahedron Lett.* **2009**, *50*, 7008–7013.

[45] J. Karolin, L. B. A. Johansson, L. Strandberg, T. Ny, *J. Am. Chem. Soc.* **1994**, *116*, 7801–7806.

[46] S. Sengupta, U. K. Pandey, *Org. Biomol. Chem.* **2018**, *16*, 2033–2038.

[47] Y. Hong, J. W. Y. Lam, B. Z. Tang, *Chem. Soc. Rev.* **2011**, *40*, 5361–5388.

[48] J. Mei, Y. Hong, J. W. Y. Lam, A. Qin, Y. Tang, B. Z. Tang, *Adv. Mater.* **2014**, *26*, 5429–5479.

[49] Y. Hong, J. W. Y. Lam, B. Z. Tang, *Chem. Commun.* **2009**, 4332–4353.

Manuscript received: May 14, 2019
Revised manuscript received: June 4, 2019
Accepted manuscript online: June 5, 2019